Stratification of colloidal aggregation coupled with sedimentation

Agustín E. González*
Instituto de Ciencias Físicas, Universidad Nacional Autónoma de México, Apartado Postal 48-3, 62251 Cuernavaca, Morelos, Mexico
(Received 13 April 2006; revised manuscript received 11 July 2006; published 19 December 2006)

One of the consequences of sedimentation in colloidal aggregation is the stratification of the system in the sense that, after a sufficiently long elapsed time, the large clusters lie preferentially at the bottom zones of the confinement prism, and the structural and dynamical quantities describing the aggregates depend on the depth at which they are measured. A few years ago a computer simulation using particles for colloidal aggregation coupled with sedimentation was proposed by the author [A. E. González, Phys. Rev. Lett. **86**, 1243 (2001)]. In that simulation, due to computational limitations, the mentioned quantities were averaged over all clusters in the prism, independently of the depth at which they were located, in order to have good statistics for the evaluation of the cluster fractal dimension and the cluster size distribution function. In this work we present a computer simulation using particles of colloidal aggregation coupled with sedimentation, for which the clusters in the simulation box represent those clusters inside a layer at a fixed depth and of arbitrary thickness in the prism. It would then be possible to compare the results with an eventual validation experiment, in which an aggregating sample is sipped out with a pipette at a fixed depth in the prism and subjected to further studies, or with a light scattering study in which the laser beam is focused at a fixed depth in the system. We confirm the acceleration of the aggregation rate, followed by a slowing down, compared with an aggregating system driven purely by diffusion (DLCA). In the present system, the large clusters when drifting downwards sweep smaller ones, which in turn occlude the holes and cavities of these large clusters, increasing in this way their compacticity. We also confirm that (i) in some cases of sedimentation strengths and layer depths, the mean width (perpendicular to the gravitational field direction) and the mean height of the large settling clusters scale with the size as a power law, with the same scaling power, in some range of cluster sizes. This leads to self-similar clusters with an appreciably higher fractal dimension (d_f) than the d_f of DLCA clusters, a case that we called the "sweeping scaling regime" in earlier works. However, the present system is much richer than DLCA in that (ii) there are some other cases for which the parallel and perpendicular scaling powers differ, leading to anisotropic self-affine clusters. (iii) There are further cases for which only the mean width *or* the mean height scale as a power law, leading again to anisotropic clusters. Finally, (iv) there are still some cases for which neither the mean width nor mean height scale as a power law with the size. In the last (ii), (iii), and (iv) cases the large settling clusters are anisotropic and non-self-similar, and a fractal dimension cannot be defined for them, as found recently by some other authors for case (iii); however, their "compacticity" should be greater than that for DLCA clusters, in a yet undefined way.

DOI: 10.1103/PhysRevE.74.061403 PACS number(s): 61.43.Hv, 05.10.Ln, 82.70.Dd

I. INTRODUCTION

Aggregation phenomena have been studied since the beginning of the last century [1,2]. In more recent years, after the proposal of a single-aggregate diffusive model by Witten and Sander [3], and more adequate for our purpose of colloidal aggregation, after the development of a diffusive model for cluster aggregation, simultaneously made by Meakin [4] and by Kolb *et al.* [5], the number of works dealing with the aggregation of particles has increased considerably. Aggregation of particles and clusters is still of great interest due to the number of applications it has in chemical engineering, materials science, biology, and atmospheric research [6,7]. Notwithstanding this fact, almost all the research in colloidal aggregation has been done neglecting the sedimentation that takes place when the large aggregates are pulled down by the gravitational force, in those cases for which there is an appreciable difference between the density of the colloidal particles and the density of the solvent. It has been only in the past 10–15 years [8–22] that researchers have paid increasing attention to such phenomenon, when the aggregation of diffusing clusters is coupled with the sedimentation experienced preferentially by the large aggregates.

The coupling between cluster diffusion and sedimentation in colloidal aggregation leads to much richer, nontrivial phenomena, that abound in many natural and industrial processes, than the much more studied colloidal aggregation problem driven purely by diffusion. Among the many examples we can cite the clearing or clarifying of liquids, the settling of bacteria clusters in quiet water, the aggregation and deposition of asphaltenes in crude oil, and a number of precipitation techniques employed by the chemical industry. With the addition of salts or flocculants, which screen the electrostatic repulsion between the particles or which establish bridges between them, it is induced the aggregation of the particles into clusters, which themselves collide with other clusters, stick together and become larger. Initially, the aggregates are small and essentially move by diffusion. As the aggregation proceeds, the settling velocity of the large aggregates becomes significant, and a mechanism for the movement of these large clusters appears. As the sedimenta-

*Electronic address: agus@fis.unam.mx

tion velocity of the small aggregates is lower than that for the larger ones, these large clusters catch up with the smaller ones, actually sweeping them and becoming in the process larger and larger. As a result, the hitting rate between aggregates increases, which leads to an acceleration of the aggregation kinetics. However, as the colloidal matter in the bulk becomes more and more scarce, due to the deposition of the large aggregates on the bottom of the sample, the aggregation kinetics eventually slows down, as we will see below. In the final state and for the nongelling cases (low concentrations), the system is composed of a tenuous sediment on the bottom and a clear fluid above.

Historically, the irreversible aggregation processes where neither sedimentation effects nor cluster breakup occur have been classified depending on the sticking probability after collisions [23–26]. When this probability is one, the particles and clusters diffuse freely and aggregate at the first contact between them. The aggregation is then termed diffusion-limited colloidal aggregation (DLCA). If, on the other hand, a large number of encounters are needed to generate a new cluster, the aggregation is called reaction-limited colloidal aggregation (RLCA). Our current knowledge in three dimensions [27,28] of the DLCA process is as follows. (a) The fractal dimension d_f of the clusters in the dilute limit is about 1.80. However, it increases from this value as a square root of the particle concentration. (b) The number-average $[S_n(t) \equiv \Sigma_s N_s(t) s / \Sigma_s N_s(t)]$ and weight-average $[S_w(t) \equiv \Sigma_s N_s(t) s^2 / \Sigma_s N_s(t) s]$ cluster sizes grow linearly with time in the dilute limit $S_n(t) \sim t^{z'}$ and $S_w(t) \sim t^z$, with $z = z' = 1$. Here $N_s(t)$ is the cluster size distribution function that gives the number of clusters with s particles at time t. Once again, the exponents z and z' increase from one as a square root of the particle concentration. (c) The cluster size distribution $N_s(t)$ is bell shaped in the late stages of the aggregation process.

Experimentally, this new problem of aggregation coupled with sedimentation has been studied more extensively by Allain and collaborators [9–11,13,14,16], who found an increase in the d_f of the large, settling aggregates (reaching values as high as 2.2) [10,11]. They attributed this increase in the d_f of the large clusters to a restructuring mechanism, due to the hydrodynamic stresses felt by their branches when they drift downwards. They also found the large settling aggregates to be nonrotating. See Refs. [17,21] for a possible explanation of this behavior.

On the simulational side and in our first works [15,17,21] that consider both sedimentation and deposition (through a rarefaction of colloidal matter in the bulk), due to computational limitations, the structural (d_f) and dynamical quantities [basically $S_w(t)$] were obtained from averages over the clusters inside the aggregating prism, independent of their vertical position. This assumption was necessary in order to have good statistics for the evaluation of the averages of highly fluctuating quantities. However, the colloidal aggregation problem coupled with sedimentation *is not* homogeneous on the vertical direction. In Fig. 1 we are reproducing Fig. 1 of Chap. III of Ref. [9] (the horizontal straight lines were added by the present author). In their system, the Calcium Carbonate spherical colloidal particles were of a diameter of

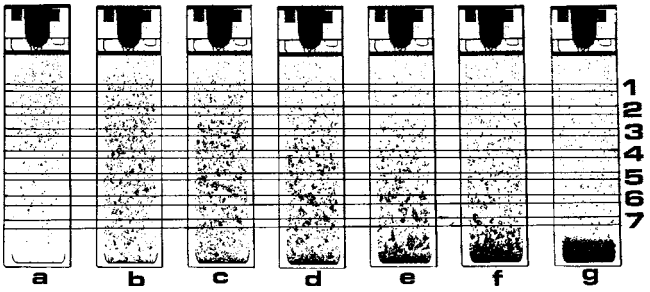

FIG. 1. The states at different times of a calcium carbonate aggregating suspension of spherical particles, for the following times: (a) 5 min 20 s, (b) 6 min 20 s, (c) 6 min 40 s, (d) 7 min, (e) 7 min 20 s, (f) 7 min 40 s, and (g) 8 min (from Ref. [9]).

0.07 μm; therefore, they cannot be optically seen unaggregated, and even the smallest points shown are actually clusters of many particles. The confinement prism was 1 mm in thickness, 10 mm wide, and of a height of 50 mm, while the volume fraction ϕ was set to the value of 0.001. The prism was illuminated from behind in such a way that what we actually see are the shadows of the clusters. We can clearly see in this figure that, for a sufficiently long time, the large clusters lie preferentially deeper than the smaller ones, which leads to a stratification of the system, as mentioned. Moreover, in each of the seven sublayers shown, we can also see that the average cluster size increases with time and peaks at a certain time, diminishing afterwards. The deeper the layer is, the longer the time it takes to peak and the higher the value at which it peaks.

In Refs. [18,19] the authors divided the aggregating prism in three nonoverlapping regions of equal height: top, middle, and bottom, in an effort to consider the dependence on the z coordinate of the aggregating quantities, and performed the much needed averages over all clusters in each of the regions. Unfortunately, their aggregation prism was not of a height big enough, in order to see a substantial increase of the clusters d_f, as we have shown [21]. More recently, in Ref. [22], the authors considered a two-dimensional lattice model for aggregation coupled with sedimentation; that is, they considered the z coordinate on the direction of the field and only one horizontal coordinate. They found that, for some cases of high sedimentation strengths and within some range of sizes, the mean width of the large settling clusters scaled as a power law with the cluster size while the mean height did not, leading to anisotropic clusters for which a fractal dimension could not be defined. To proceed further in this problem, what we actually need is an algorithm capable of proportioning the *average* aggregation quantities at a *fixed* depth in the prism, and consider a good number of cases of sedimentation strengths and layer depths. In Ref. [29] such an algorithm was presented in the form of a letter in which, by the nature of its size, it was not possible to show all the different cases of sedimentation strengths and depths, that lead to different behaviors in this problem. The purpose of the present article is to fill this gap, and consider in detail a number of interesting cases of sedimentation strengths and depths, with such algorithm.

The organization of this article is as follows. In Sec. II we give an explicit description of the model and algorithm used

in the simulations, and also set the values of the parameters considered. The dynamics of the aggregation is studied in Sec. III, where we first present in Sec. III A the weight-average cluster size as a function of time. We will see that this quantity behaves in accordance to what we saw in Fig. 1. The time evolution of the number of clusters in the different layers $[N_c(t)]$ will be shown in Sec. III B, where the slowing down after the speeding up of the aggregation will become evident. To end up with the dynamics, the evolution of the particle volume fraction ϕ in the layers will be presented in Sec. III C. The cluster structure for all cases considered will be studied in Sec. IV. In Sec. IV A we first present those cases for which the large settling clusters are still isotropic, the mean width and the mean height scaling as a power law with the cluster size (N), with the same scaling power and within a certain range in sizes. It is therefore possible to define a cluster fractal dimension, which results appreciably higher than the DLCA d_f. Those cases correspond to what we called the "sweeping scaling regime" in earlier works [21,29]. In Sec. IV B we will present a case for which the mean width and the mean height of the large settling clusters again scale as power laws with N, but with different scaling powers; this leads to anisotropic, self-affine clusters, for which it is not possible to define a d_f. The cases for which the mean height of the big drifting clusters scales as a power law with N, while the mean width does not, and vice versa, with no possibility to define a cluster d_f, are considered in Sec. IV C. In Sec. IV D are considered those cases for which a settling clusters regime disappears, leaving over only a quasi-DLCA regime, which occurs generally for very shallow depths and/or for not so shallow depths but with a low sedimentation strength. In such cases, the large clusters do not have the possibility to do a substantial sweeping of the small clusters. The "quasi" means that the large clusters still do some sweeping, increasing in this way a little bit their d_f from the DLCA value. To finish the structural studies, in Sec. IV E are shown the cases of very high sedimentation strengths, for which the clusters become very soon anisotropic. In those cases, the scaling as a power law of the mean width and mean height with N is lost, even for small clusters, marking the disappearance also of the quasi-DLCA regime. Finally, in Sec. V the paper is ended with some discussions and conclusions of the results shown.

II. THE MODEL

Let us consider the sedimentation velocity v_s experienced by a cluster of N spherical particles of radius a and mass m_0:

$$v_s = \frac{m_0(1-\rho/\rho_0)gN}{f} = \frac{m_0(1-\rho/\rho_0)g}{k_BT}DN, \qquad (1)$$

where ρ_0 is the particle density, ρ is that of the suspension fluid, $f=6\pi\eta R_g$ is the cluster's friction coefficient, $D\left(=\frac{k_BT}{f}\right)$ is its diffusion coefficient, R_g is its radius of gyration, η is the solvent viscosity, and T is the temperature. Note that rigorously we should have written $f=6\pi\eta R_H$, where R_H is the hydrodynamic radius of the cluster, which was shown experimentally to be proportional to the radius of gyration [30]. Since in all the formulas for moving the clusters in the algorithm, including the comparison of the two Monte Carlo (MC) step times (see below), we obtain the ratio of two radii ($R_{g\ \min}/R_g$ or $R_g/R_{g\ \max}$), the constants of proportionality cancel out allowing us to use the R_g in the definition of the friction coefficient. This R_g can be calculated directly in the simulations for each cluster. Let t_0 be the time for which the cluster diffuses a particle diameter $(d=2a)$, that is, $t_0=2a^2/3D$. During the same time, the cluster drifts a distance $d_s=v_st_0=\frac{1}{3}\mathrm{P_e}Nd$, where $\mathrm{P_e}\equiv m_0(1-\rho/\rho_0)ga/k_BT$ is the Peclet number of the individual colloidal particles in the fluid. The Peclet number gives the sedimentation strength felt by the particles, being a number much smaller than one for most colloidal systems with a size generally smaller than 1 μm. It is in fact not difficult to show that if the colloidal particles are 1 μm in diameter $1-\rho/\rho_0$ is less than but of the order of unity, and T is room temperature, P_e is of the order of unity. However, if the diameter is 0.1 μm such quantity is of the order of 10^{-4}, while if the diameter is 10 μm, P_e goes as high as 10^4. Therefore, 1 μm marks the transition between diffusive and drifting behavior for individual particles, with density different from that of the medium.

The main difficulty with the present aggregation problem is to simulate systems large enough, in the shape of a prism, with a height big enough in order to study the big depths (in units of the particle diameter) that are considered in the experimental systems. Moreover, the width of the prism also has to be sufficiently large to allow for the formation of the big clusters, that are preferentially experiencing the sedimentation due to gravity. The simulation of such a system would be computationally unmanageable due to its enormous size. To overcome this difficulty, we consider two cubic lattices of lattice spacing d (the diameter of the particles). The first one has the shape of a square prism of height H and variable lateral size, with periodic boundary conditions on the x and y directions, that mimics the actual experimental prism. The second one has the shape of a cube of lateral size L, with periodic boundary conditions on the three spatial directions, that represents a layer of the square prism centered at the integer depth Z measured from the top of the prism, and of thickness Δ which is taken in multiples of two (see Fig. 2). Now, periodic boundary conditions applied in all three spatial directions imply no spatial variations inside the cube. This is the reason why the thickness Δ will be chosen much smaller than the depth Z at which we are focusing. The variations with the depth are considered by the different taking out probabilities, which depend on the depth Z and the thickness Δ, as we will see below. Note how this is different from the previous algorithm [15,17,21], in that the lattice with the shape of a cube there represented the whole prism of height H. Inside such lattices we have clusters made of nearest-neighbor lattice cells that are diffusing randomly in the six spatial directions, sedimenting downwards and aggregating after encounters (attempts to overlap). The simulations are actually performed in the lattice with the shape of a cube, where as is usual with the periodic boundary conditions, if a cluster leaves the cube through one of the boundaries it enters from the opposite side. We would like to consider now, for each cluster, an integer quantity Z_s which is measured in the prism as the vertical distance from the uppermost initial

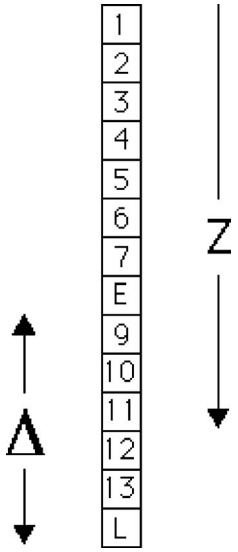

FIG. 2. A schematic representation of the square lattice prism: Each of the squares represents a layer of unit thickness in the prism. Here we are describing a case for which the depth of the analyzed layer is $Z=11$, while the thickness is $\Delta=6$. If the center of any cluster is at the cell number 8, labeled with the letter E, it will enter into the layer after a sedimentation step, while if it is at the cell number 14, labeled with the letter L, it will leave the layer after such step.

particle that will eventually belong to the given cluster, to the center of this cluster — defined at a suitable cell — at the present position in the prism. At the initial time there are only single particles randomly positioned which, of course, have $Z_s=0$. To calculate this quantity in the simulational cubic box, whenever a cluster moves in the z direction a lattice spacing d, the quantity Z_s is updated, which furnishes us with the total distance in units of d that the cluster has moved downwards (taking into account the movement of all its ancestors; i.e., the largest of the two quantities Z_s of the two colliding clusters is generally but not always inherited to the new formed cluster after a merging. A technical detail: as the Z_s after a merging is measured up to the center of the new formed cluster, it is possible that sometimes the cluster with the smaller Z_s, plus the vertical distance from its center to the center of the new cluster, would produce the largest value of the Z_s for the new formed cluster. In this case this is the Z_s that we take for the new cluster).

Every time a cluster is picked at each MC step we check whether it diffuses and/or sediments downwards a lattice spacing (see below). In the last case, to simulate the clusters inside the above mentioned layer of thickness Δ of the prism, of all the $Z+\frac{\Delta}{2}-Z_s\geq 1$ possible layers of unit thickness where the center of this cluster can be, only at the lowest layer — with the position $Z+\frac{\Delta}{2}$ — would be taken out of the layer of thickness Δ by a sedimentation step, while if it is at the layer at $Z-\frac{\Delta}{2}$ the sedimentation step would take it inside. Therefore, if Z_s has not grown enough for such cluster such that $Z-\frac{\Delta}{2}-Z_s\geq 1$, it is not taken out of the box, assuming that it has the same probability to be on either of those two layers of unit thickness of the prism. On the other hand, if $Z-\frac{\Delta}{2}-Z_s\leq 0$, the cluster cannot be at the position $Z-\frac{\Delta}{2}$ and is therefore taken out of the box with probability $1/\left(Z+\frac{\Delta}{2}-Z_s\right)$. In this way we are simulating the depletion of colloidal matter inside the different layers in the aggregation prism, due to sedimentation.

We pick the MC step time to not allow a cluster to move more than one lattice spacing. Define $\Delta t_{\mathrm{dif}}\equiv d^2/6D_{\max}$ as the time taken by the most mobile cluster to diffuse one lattice spacing. Also, let $\Delta t_{\mathrm{drif}}\equiv d/v_s^{\max}$ be the time taken by the largest cluster to sediment downwards one lattice spacing. The algorithm is as follows.

(a) If $\Delta t_{\mathrm{drif}}<\Delta t_{\mathrm{dif}}$ then we have the following.

(1) pick a cluster in a cyclic way. That is, the clusters are numbered and, after having chosen a cluster, the next cluster to choose will be the following in the list, given that sedimentation is a deterministic process.

(2) The time is increased by $\Delta t_{\mathrm{drif}}/N_c(t)$, where the division by $N_c(t)$ comes from the fact that after a cycle, when all the clusters have been picked once (assuming that no merging took place), the time increase is Δt_{drif}.

(3) The quantity $\Delta t_{\mathrm{drif}}\, v_s/d$ is calculated and the result is added to a real variable associated to that cluster, that we called Z_{sed}. The initial values of the variables Z_{sed} of all the clusters are equal to zero. If the sum is greater than one, the cluster is moved downward one lattice spacing and the new value of the variable becomes the remainder of the sum modulo one; the variable Z_s is consequently updated to its previous value plus one and the cluster is taken out of the box with probability $1/\left(Z+\frac{\Delta}{2}-Z_s\right)$, only if $Z-\frac{\Delta}{2}-Z_s\leq 0$. We then go back to the starting situation to calculate Δt_{dif} and Δt_{drif}.

(4) If the cluster is moved but not taken out, we check for overlapping with other clusters, in which case the moved cluster is taken back to its original position and the overlapping clusters are merged (which implies a sticking probability equal to 1). We then go back to the starting situation to calculate Δt_{dif} and Δt_{drif}.

(5) If the cluster movement does not lead to overlap, it now moves one lattice spacing in a random direction, with probability $(\Delta t_{\mathrm{drif}}/\Delta t_{\mathrm{dif}})(D/D_{\max})$. The factor $\Delta t_{\mathrm{drif}}/\Delta t_{\mathrm{dif}}$ (<1) modifies the usual diffusion probability of a cluster [4,5], due to a MC step time smaller than Δt_{dif}. If it moves along the z direction, Z_s is consequently updated. We now check for overlapping, etc., as in point (4).

(6) If the cluster movement does not lead to overlap, the procedure is continued at point (1).

(b) If, on the other hand, $\Delta t_{\mathrm{dif}}\leq\Delta t_{\mathrm{drif}}$ we follow the same procedure (a), with the difference that everywhere we find Δt_{drif} in a formula, it is replaced by Δt_{dif}.

The volume fraction was fixed at the value $\phi=0.001$. We considered four depths: $Z=500$, 5000, 50 000, and 500 000, measured in terms of the diameter, and one single $\Delta=100$. For each of those depths, five Peclet numbers were considered $P_e=0.0001$, 0.001, 0.01, 0.1, and 1.0. In turn, for each Peclet number, a series of 10 simulations of 274 625 particles were made (corresponding to a box size of 650 diameters), in order to have enough statistics to evaluate the structural and dynamical quantities.

III. DYNAMICS

A. The evolution of $S_w(t)$ in the layers

In Fig. 3 are shown the weight-average cluster sizes as a function of time $S_w(t)$ for the Peclet numbers (a) 1.0, (b) 0.1, (c) 0.01, and (d) 0.001. As we can see in the figures, S_w increases with time, peaks at a certain time, and diminishes afterwards, a behavior that is in accordance to what we saw qualitatively in Fig. 1. We also note in all four figures that the deeper the layer we are considering, the longer the time it takes to peak and the higher the value at which it peaks, again in correspondance with Fig. 1. The peak in the S_w indicates that for each Peclet number and for each layer there is a typical maximum cluster size above which no aggregates can be found, where by typical we mean the order of magnitude. This typical maximum size increases with the deepness of the layer, for a given Peclet number. In Figs. 3(c) and 3(d) we present a phenomenon that does not appear in the experiments, namely, that for low Peclet numbers and very deep layers, some clusters become so big (on the order of 10^5 particles) that they span our finite cubic box of lateral dimension of 650, and the system gels. Therefore, the simulations had to be stopped at the gel point. That is why, in curve d of Fig. 3(c), and in curves c and d of Fig. 3(d), the decrease of S_w does not appear after the peak but only the increase. This did not occur in the experimental system because of two possible reasons: (i) even the shortest side of their parallelepiped (thickness) was of ~14 300 particle diameters in size and (ii) there is a limiting size $R_{\max}$ above which the aggregates do not grow [11] due to cluster fragmentation, which is not considered in the present model. However, their value of $R_{\max} \simeq 0.5$ mm [11] makes us believe that it is the finite size of our cubic lattice the one responsible for gelation, because our clusters are well below their $R_{\max}$ in units of the particle diameter.

We confirmed the speeding up of the aggregation rate as compared with the DLCA case, now for a fixed depth when this depth is big enough, due to the increasing pace at which the big clusters drift downwards, catching up more and more small clusters below them and increasing in this way the hitting rate [15,17,21]. The speeding up is illustrated in Fig. 4, where we are now plotting again $S_w(t)$ such that all the curves for a given depth and the different P_e's are shown in the same graph. In Fig. 4(a) we show the S_w curves for the $Z=500$ layer, while in Figs. 4(b)–4(d) are shown the curves for the $Z=5000$, 50 000, and 500 000 layers, respectively. As can be seen in Figs. 4(b)–4(d), the curves for all Peclet numbers different from zero depart from the DLCA curve, increasing at a higher rate. The higher the Peclet number considered, the sooner the curve starts to depart. Note again the existence of some curves with no maximum because they were cut at the gel point, which occurred generally for low P_e's and big depths. More precisely, gelation occurred for $Z=5000$ with $P_e=0.0001$; for $Z=50\,000$ with $P_e=0.0001$ and 0.001; and finally, for $Z=500\,000$ with $P_e=0.0001$, 0.001, and 0.01. For the very shallow depth of 500, there was no increase of the S_w curves above the DLCA one, except for a very slight increase of the curve for $P_e=1$. This indicates that for such depth the clusters did not have the opportunity to do a substantial sweeping in that distance, therefore preventing the acceleration of the kinetics.

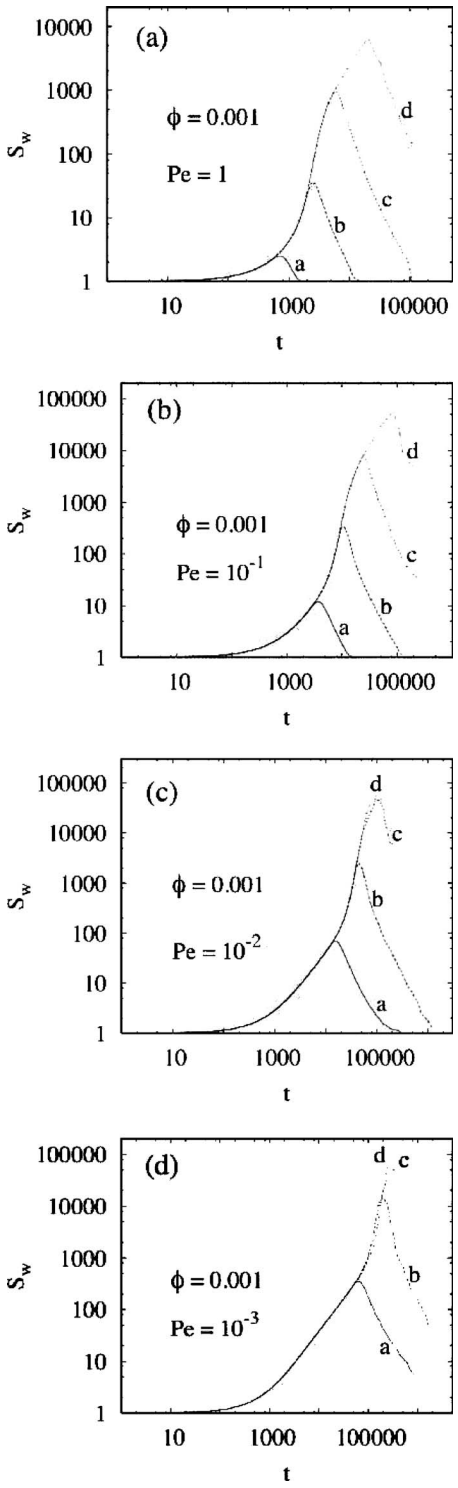

FIG. 3. A log-log plot of the time evolution of the weight-average cluster size S_w for the Peclet numbers (a) $P_e=1$, (b) $P_e=0.1$, (c) $P_e=0.01$, and (d) $P_e=0.001$. In all four figures the labels of each of the curves a, b, c, and d correspond to the following depths: 500, 5000, 50 000, and 500 000, respectively.

For times before the S_w reaches its maximum, there is essentially no depletion of colloidal mass in the layers, as we

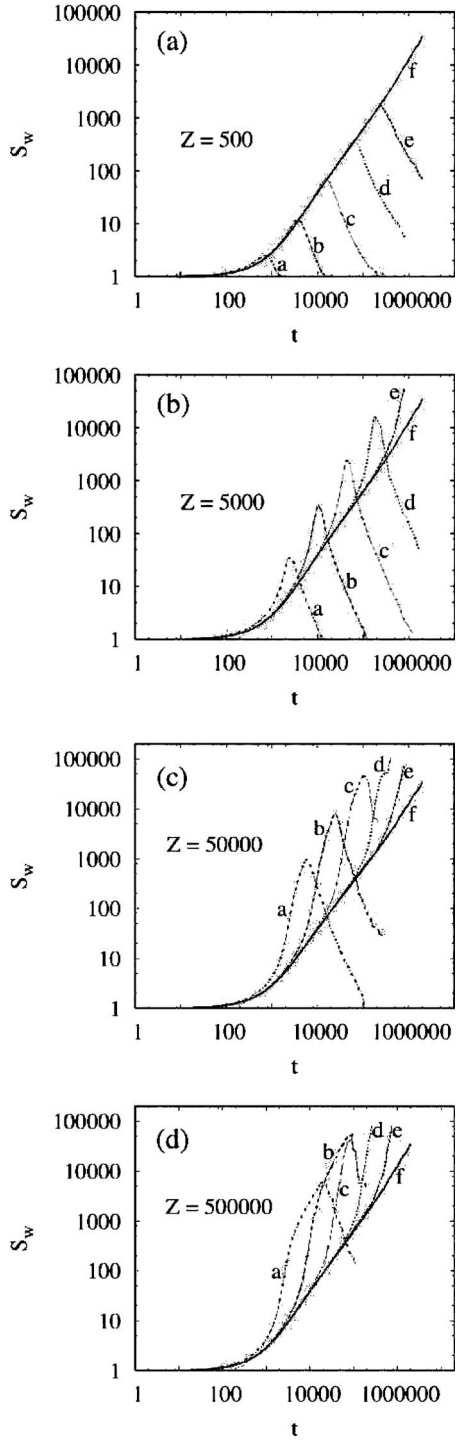

FIG. 4. A log-log plot of the time evolution of the weight-average cluster size S_w for the layers at (a) $Z=500$, (b) $Z=5000$, (c) $Z=50\,000$, and (d) $Z=500\,000$. In all four figures the labels of each of the curves a, b, c, d, e, and f correspond to the following Peclet numbers: 1.0, 0.1, 0.01, 0.001, 0.0001, and 0.0 (DLCA simulation), respectively.

will see below, because the departing of clusters through the boundary below is counterbalanced by the arrival of clusters through the boundary above. However, as soon as the S_w reaches its maximum and it is possible to find typical maximum size aggregates in a given layer, no counterbalance would occur when these typical maximum size clusters leave the layer from below, because it is not possible to find aggregates of that size in the layers above. The layer then starts to become rapidly depleted of these big clusters. Afterwards, as the time proceeds, the layer is depleted now of smaller clusters, for the same reason. All this forces the S_w to diminish rapidly, as seen in Figs. 3 and 4. Due to both effects: (i) the absence of large sweeping clusters and (ii) the rarefaction of colloidal matter in a given layer, there is a reduction of the hitting rate, with the consequent slowing down of the kinetics.

B. The evolution of $N_c(t)$ in the layers

The slowing down of the aggregation rate *after* the speeding up is also seen in the curves for the number of clusters in the layers as a function of time $N_c(t)$. Note that in order to start with the same number of initial particles as we are considering here, and due to the thickness of our layers equal to 100 lattice spacings, the transversal area of the prism should be of 2 746 250, in order for the volume of the layer to be equal to that of the cubic box: 650^3. This corresponds to a square prism of lateral size of about 1657 lattice spacings.

In Fig. 5 we plot the number of clusters in the layers as a function of time, $N_c(t)$. In Fig. 5(a) are shown the N_c curves for the $Z=500$ layer, while in Figs. 5(b)–5(d) are shown the curves for the $Z=5000$, $Z=50\,000$, and $Z=500\,000$ layers, respectively. In each of the figures, the curves for $P_e=1.0$, 0.1, 0.01, 0.001, 0.0001, and 0.0 are labeled with the letters a, b, c, d, e, and f, respectively. As we can see in all four figures, there is a higher decrease in the number of clusters as a function of time for all P_e'$s \neq 0$, as compared with the case $P_e=0$ (DLCA simulation). The higher the Peclet number, the sooner the curve starts to depart from the DLCA curve. This higher decrease comes again from the higher hitting and aggregation rate when the big settling clusters are sweeping the small clusters and single particles that find below them. However, for not so shallow depths as in Figs. 5(b)–5(d), and for the cases where no gelation takes place, we can clearly see another phenomenon taking place, namely, that the decrease slows down, which is signaled by the wiggles in the $N_c(t)$ curves. As mentioned, the slowing down in the decrease of $N_c(t)$ is due to lower hitting and aggregation rates between clusters. Nevertheless, after this slowing down, the decrease of $N_c(t)$ starts up again at a higher rate, this time coming mainly from the rarefaction of colloidal mass (clusters) in the layer. The absence of wiggles in the layer at $Z=500$ and for high P_e's is probably due to the fact that the layer is rapidly depleted of colloidal matter in a very short time, and we cannot even talk about hitting and aggregation rates.

C. The evolution of the particle density in the layers

In Fig. 6 we show the volume fraction ϕ as a function of time in the layers for (a) $Z=500$, (b) $Z=5000$, (c) $Z=50\,000$, and (d) $Z=500\,000$, and for all the Peclet numbers studied. In view of the way that the depletion of colloidal mass in the layers was calculated, this $\phi_{\text{layer}}(t)$ is actually an

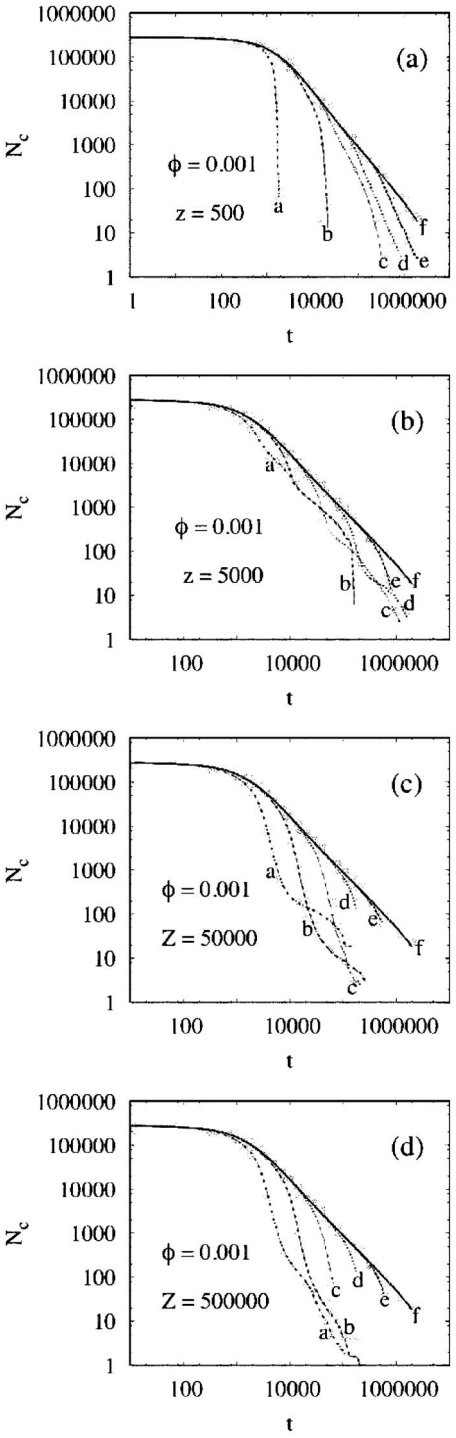

FIG. 5. A log-log plot of the time evolution of the number of clusters in the layers $N_c(t)$ for the layers at (a) Z=500, (b) Z =5000, (c) Z=50 000, and (d) Z=500 000. In all four figures the labels of each of the curves a, b, c, d, e, and f correspond to the following Peclet numbers: 1.0, 0.1, 0.01, 0.001, 0.0001, and 0.0 (DLCA simulation), respectively.

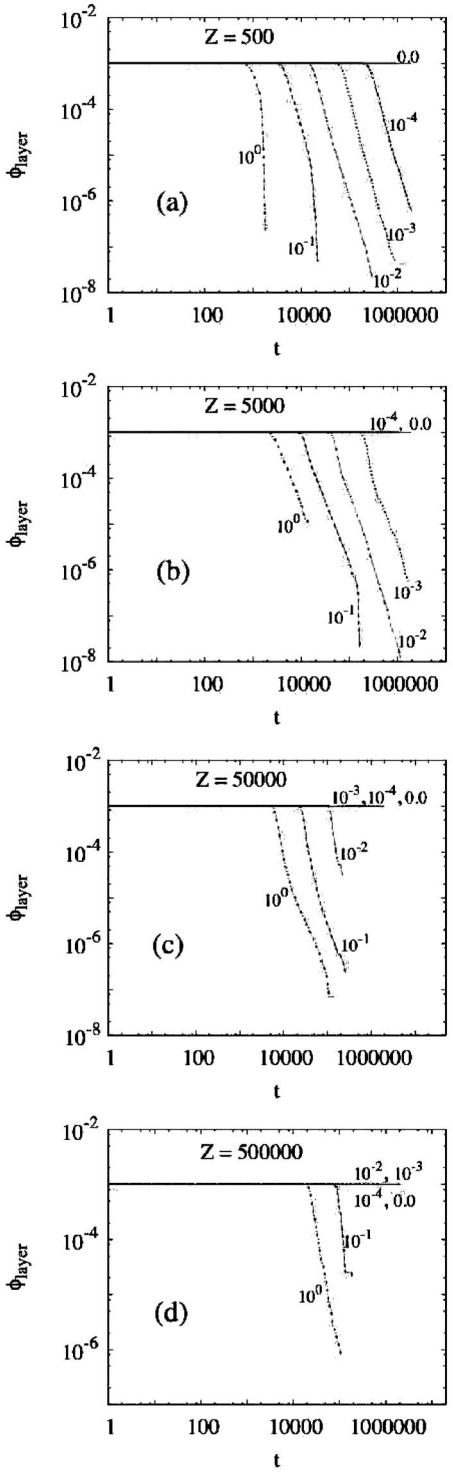

FIG. 6. The time evolution of the particle density in the layers ϕ_{layer} for the depths at (a) Z=500, (b) Z=5000, (c) Z=50 000, and (d) Z=500 000. In all four figures each of the curves is labeled with the corresponding Peclet number.

average density (which is in fact what we want), absent of fluctuations coming from the Brownian motion of the clusters. As we can see, all the curves start at the initial value ϕ=0.001 and continue with that value for a certain elapsed time, after which they decrease rapidly. The higher the Peclet number, the sooner the curve starts to depart from the initial value. The main reason for showing these plots is to corroborate that the time of departure from ϕ=0.001 corresponds roughly to the time for which $S_w(t)$ reaches its maximum value, as can be seen in Fig. 4. This indicates that indeed the

rarefaction of colloidal matter in the layers, starting with the typical maximum size clusters, with the consequent slowing down of the aggregation rate, comes *after* the speeding up.

IV. STRUCTURE

The addition of a gravitational field on the vertical z direction in the colloidal aggregation problem, felt preferentially by the big clusters, introduces some degree of anisotropy in the structure of these clusters, as we will see below. It is important to mention at this point that the clusters in colloidal aggregation driven purely by diffusion (DLCA) are inherently anisotropic [31–33], in the sense that the radius of gyration tensor has three different eigenvalues, and the average ratio of the largest to the smallest eigenvalue is different from one. This was tested in several monodisperse models in Refs. [31,32] and by a more realistic model of clusters diffusing and aggregating in a box in Ref. [33]. However, the diagonal components of this tensor R_{gx}, R_{gy}, and R_{gz}, defined as $R_{gx}^2 \equiv \Sigma_{i=1}^{N}(x_i - x_{cm})^2/N$, etc., when averaged over many clusters of the same size (N), have to coincide given that the orientation in space of their major axes varies randomly without a preferential direction. In this formula x_i is the x component of the position of particle i of the cluster and x_{cm} is the x component of the position of its center of mass. The radius of gyration R_g of the cluster will then be given by $R_g^2 = R_{gx}^2 + R_{gy}^2 + R_{gz}^2$. Here we would like to consider a different type of anisotropy, induced by the addition of the gravitational field, in which the average values of R_{gx} and R_{gy} over clusters of roughly the same size are equal, up to the statistical uncertainties, but different to the average value of R_{gz}. It is therefore necessary to define and study some anisotropy measures of the clusters before trying to do a radius of gyration vs size, log-log analysis, in order to see if it is possible to extract a fractal dimension from such plots. Let us define the anisotropy measures $A_{xz} \equiv \langle R_{gx}/R_g \rangle / \langle R_{gz}/R_g \rangle$ and $A_{yz} \equiv \langle R_{gy}/R_g \rangle / \langle R_{gz}/R_g \rangle$, where the average values are calculated over all clusters inside segments of constant magnitude in the logarithmic size scale N. Note that for isotropic clusters, the measures A_{xz} and A_{yz} should be equal to one, up to the statistical uncertainties. After studying the A_{xz} and A_{yz} quantities, we will make plots of not only $\langle R_g \rangle$ vs N, but also of $\langle R_{gx} \rangle$ vs N, $\langle R_{gy} \rangle$ vs N, and $\langle R_{gz} \rangle$ vs N, to find any regions for which we have a power law scaling of those quantities. Here again the averages of the different radii are made over the same segments of constant magnitude in the logarithmic size scale. We have found a whole variety of behaviors for the structure of the clusters in this problem, depending on the sedimentation strength (P_e), the layer depth (Z), and the region of sizes considered. Generally speaking, the four radii (R_{gx}, R_{gy}, R_{gz}, and R_g) scale as a power law with N, with the same scaling power, for the small, non-settling clusters, except for a number of cases with a high sedimentation strength: $P_e = 1.0$ for all depths and $P_e = 0.1$ for $Z = 500\,000$. In those cases of cluster isotropy it is therefore possible to define a cluster fractal dimension, This behavior shall be called the quasi-DLCA regime, where the "quasi" means that, as there is still some sweeping of even smaller clusters, the fractal dimension is a little bit higher than the usual DLCA d_f. For the large, settling clusters, we have found cases for which the four radii again scale as a power law with N, with the same scaling power, making it possible to define a settling-clusters fractal dimension, a behavior that shall be called the sweeping scaling regime. There are, however, cases for which the scaling powers for the horizontal and vertical directions differ, obtaining therefore self-affine settling clusters. There are still some cases for which only the mean width *or* the mean height scale as a power law with N, and even further cases for which no scaling as a power law of the four radii is obtained.

A. The sweeping scaling regime

This regime is obtained at deep layers and intermediate Peclet numbers; the deeper the layer considered, the lower the P_e that can be used to attain the regime. In our studies we have found this regime for $Z = 500\,000$ with $P_e = 0.01$, 0.001, and 0.0001, and for $Z = 50\,000$ with $P_e = 0.001$. In Fig. 7 we show the case for $Z = 500\,000$ and $P_e = 0.001$. The anisotropy measure A_{yz} is first shown in Fig. 7(a), where the error bars in the graph correspond to the standard deviation of the plotted quantity. In fact, in this paper, whenever an uncertainty is given for a quantity, it correspond to the standard deviation of such quantity. As we can see, A_{yz} stays very close to one for all sizes up to about 10 000, which is therefore the upper bound in this case for trying to obtain a fractal dimension from the log-log plots of the four radii vs N. After this upper bound, the clusters become definitely oblate. It should be mentioned that for the anisotropy measure A_{xz} we obtain a quite similar plot, with the same upper bound. In Fig. 7(b) is shown the log-log plot of the average radius R_{gx} vs N. After an initial curvature, corresponding to the corrections to scaling zone for small sizes, we obtain not one but two straight lines, before the upper bound is reached. The straight line boundaries, defined by the arrows, were obtained by the usual method of expanding the left boundary to the left, first, and then the right boundary to the right, or vice versa, until the slopes produced ceased to oscillate, increasing or decreasing continuously. This means that there are two zones for which we have scaling as a power law of the R_{gx} with N, one defined by the arrows labeled a and the other by the arrows labeled b. The first one corresponds to the quasi-DLCA regime, with an inverse of the scaling power equal to $d_{fax} = 1.842 \pm 0.008$, while the second one has an inverse of the scaling power of $d_{fbx} = 2.086 \pm 0.111$. After the upper bound, the R_{gx} does not scale with N as a power law. For the average radius R_{gy} vs N a very similar plot is obtained, but this time with $d_{fay} = 1.851 \pm 0.010$ and $d_{fby} = 2.003 \pm 0.055$. The log-log plot of the average R_{gz} vs N is shown in Fig. 7(c), where we can extract the following inverses of the scaling powers $d_{faz} = 1.847 \pm 0.006$ and $d_{fbz} = 2.044 \pm 0.106$. Note, however, that this plot is dissimilar with those for R_{gx} and R_{gy} in that, after the upper bound, the points deviate downwards and not upwards from the second straight line, due to the oblate shape of the large clusters. Up to the statistical uncertainties, the scaling powers for the "a" zone coincide as well as those for the "b" zone. This means that it is therefore

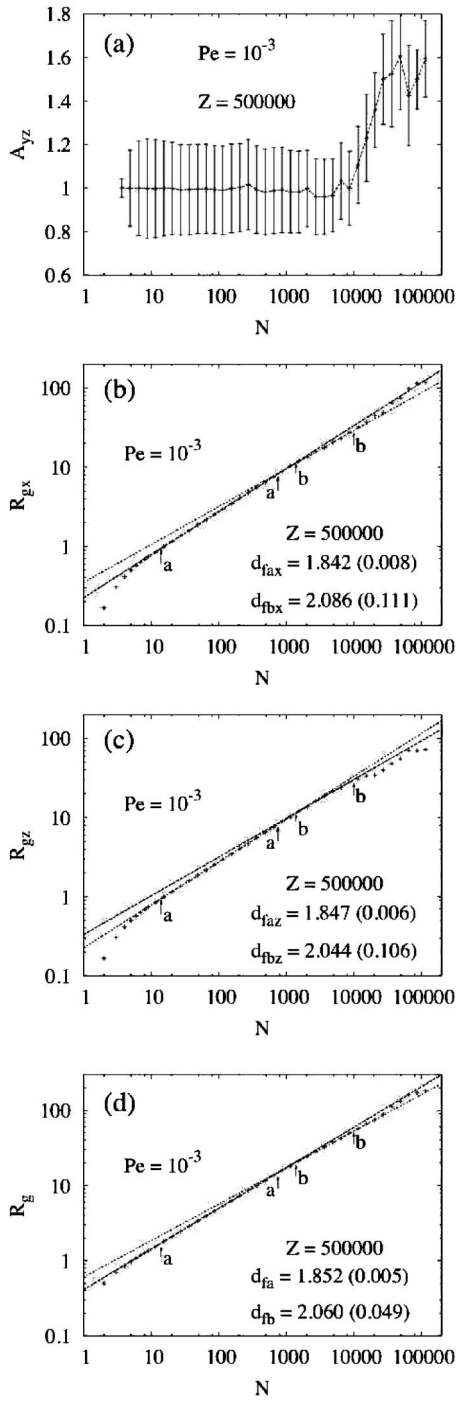

FIG. 7. All four figures correspond to the layer at $Z=500\,000$ and $P_e=0.001$. (a) A plot of the anisotropy measure (see the text) A_{yz} vs the size. (b) A plot of R_{gx} vs the size. (c) A plot of R_{gz} vs the size. (d) A plot of R_g vs the size. In (b), (c), and (d) the plotted radii are averages over all clusters inside segments of constant magnitude in the logarithmic size scale N.

possible to obtain a fractal dimension for each zone. This is done in Fig. 7(d), where we now plot the average R_g vs N. The inverses of the scaling powers provide us now with the following fractal dimensions: $d_{fa}=1.852\pm0.005$, which corresponds to the quasi-DLCA regime, and $d_{fb}=2.060\pm0.049$, corresponding to what we have called the "sweeping scaling regime" [21,29]. Note that in the graph it looks like if we can continue the second straight line for about half a decade more. This is really an artifact because, as we saw, the points after the upper bound deviate upwards for R_{gx} and R_{gy}, while the deviation is downwards for R_{gz}, making the R_g have almost no deviation, due to the equation $R_g^2=R_{gx}^2+R_{gy}^2+R_{gz}^2$.

As mentioned, for the same $Z=500\,000$ layer we have also found a sweeping scaling regime for $P_e=0.0001$ ($d_{fb}=2.170\pm0.102$) and for $P_e=0.01$ ($d_{fb}=2.049\pm0.013$). For the layer at $Z=50\,000$ there is only a sweeping scaling regime for $P_e=0.001$ ($d_{fb}=1.996\pm0.048$). For $P_e=0.0001$ and this $Z=50\,000$ layer, the clusters grow mainly by diffusion and aggregation at contact; therefore, when they are big enough to undergo a substantial sedimentation, they cannot traverse enough distance to do an appreciable sweeping of the small ones, when they reach the layer, and we are left only with quasi-DLCA clusters. It therefore seems that in order to obtain the sweeping scaling regime for lower Peclet numbers, we would need to consider bigger depths. For the shallower layers at $Z=5000$ and $Z=500$ we did not find a sweeping scaling regime for all the Peclet numbers studied.

B. A self-affine regime

We have found a self-affine regime for the case $Z=5000$ and $P_e=0.01$, shown in Fig. 8. In Fig. 8(a) we plot the anisotropy measure, this time A_{xz}, with a very similar plot for A_{yz}. In the figure we can see that A_{xz} remains very close to one up to values of $N\sim200$. After that, the clusters become a little bit elongated by noting that the A_{xz} diminishes from one by a few percent; however, it starts to increase again and crosses one at about $N\sim3000$, the clusters becoming definitely oblate after that point. Therefore, the upper bound in size for possible isotropic scaling is 200 in this case. In Fig. 8(b) we plot the average R_{gx} vs size, where we can see that, after the corrections to scaling curvature, there are two straight lines, defined by the arrows labeled "a" and "b." The inverses of the scaling powers are this time $d_{fax}=1.824\pm0.014$ and $d_{fbx}=2.064\pm0.048$. There is a very similar plot for R_{gy} vs N, but now with $d_{fay}=1.837\pm0.015$ and $d_{fby}=2.099\pm0.030$. In Fig. 8(c) is shown the plot for the average R_{gz} vs size, again with two straight lines after the corrections to scaling zone, this time with $d_{faz}=1.819\pm0.015$ and $d_{fbz}=1.901\pm0.015$. We can note that the scaling powers in the "a" zone coincide, up to the statistical uncertainties. However, although the d_{fbx} and d_{fby} inverse scaling powers are quite similar, there is no way that they can be equated to d_{fbz}, which means that the mean width and mean height scale with size as a power law, but with different scaling powers. This results therefore in self-affine clusters, with no possibility to define a fractal dimension for them. To check this, in Fig. 8(d) we plot the whole R_g vs N, where we obtain now one single straight line in the "a" zone and a continuous curvature afterwards. The inverse of the scaling power in the "a" zone is now $d_{fax}=1.842\pm0.014$, that can be defined as the fractal dimension of the clusters in this zone, which corresponds to the quasi-DLCA regime. As a final comment, the zone in which the clusters are self-affine corresponds to that zone with a somewhat elongated shape obtained in the plot of A_{xz} vs N.

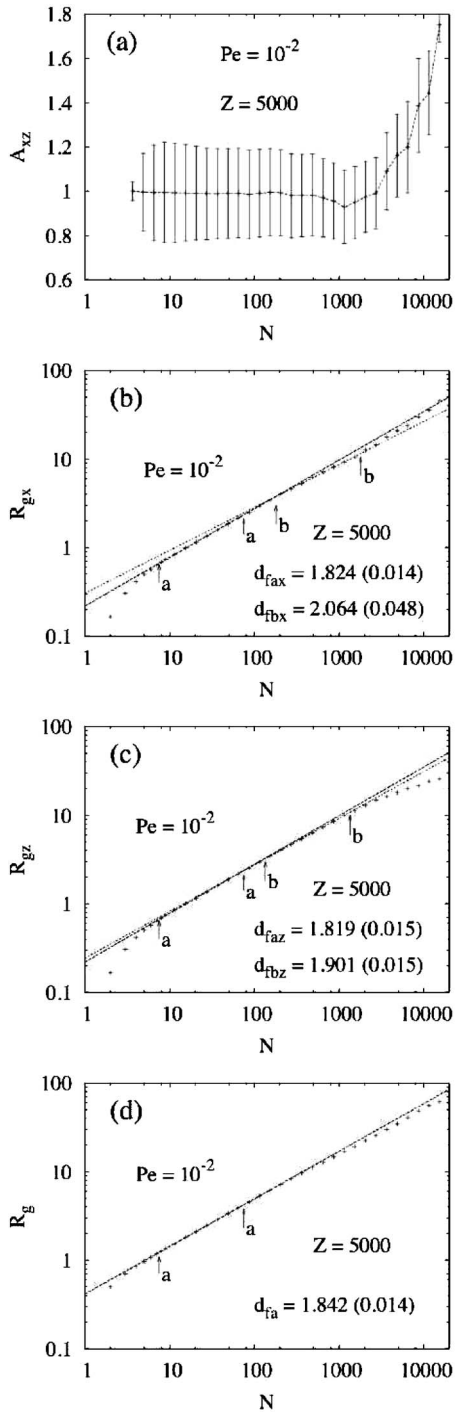

FIG. 8. All four figures correspond to the layer at $Z=5000$ and $P_e=0.01$. (a) A plot of the anisotropy measure A_{xz} vs the size. (b) A plot of R_{gx} vs the size. (c) A plot of R_{gz} vs the size. (d) A plot of R_g vs the size.

C. Cases for scaling of the mean height or the mean width only

We have found cases for which the mean height scales as a power law with N while the mean width does not and vice versa. The cases of scaling of the mean height were for $P_e=0.1$ with $Z=50\,000$ and 5000, while those of scaling of the mean width were for $P_e=0.01$ with $Z=50\,000$, and for $P_e=0.1$ with $Z=500$. In Fig. 9 we show the case $P_e=0.1$ with $Z=50\,000$. In Fig. 9(a) we can see that the anisotropy measure A_{xz} decreases very soon from one, as in all cases with a high Peclet number as we will see below, reaching values around 0.8, which indicates somewhat elongated clusters. Afterwards it starts increasing very rapidly, crossing one and reaching values close to 3.0, which indicates this time very oblate clusters. A very similar plot was found for A_{yz}. In these cases of high P_e's, the quasi-DLCA regime disappears, hidden in the curvature of the zone of the corrections to

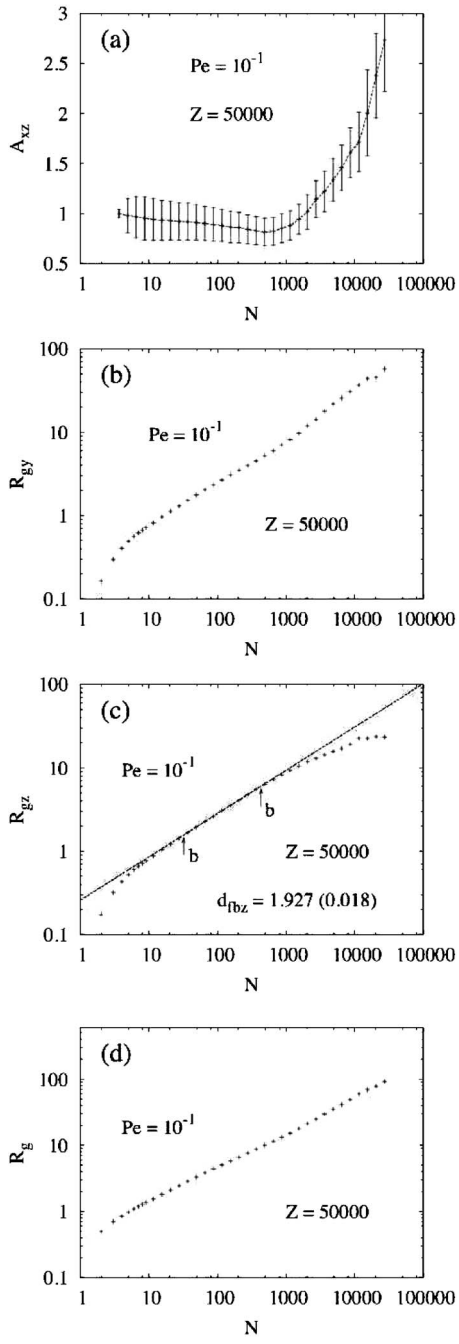

FIG. 9. All four figures correspond to the layer at $Z=50\,000$ and $P_e=0.1$. (a) A plot of the anisotropy measure A_{xz} vs the size. (b) A plot of R_{gy} vs the size. (c) A plot of R_{gz} vs the size. (d) A plot of R_g vs the size.

scaling. However, for the settling clusters we can see that there is no scaling as a power law of the average R_{gy} vs size, as shown in Fig. 9(b). The graph is all curved, with no possibility to define a straight line. A quite similar plot is obtained for the average R_{gx} vs size. Notwithstanding this, in Fig. 9(c) we can clearly see a zone of the settling clusters with a well defined straight line, which indicates scaling as a power law of the average R_{gz} vs N. The inverse of the scaling power was found as $d_{fbz}=1.927\pm0.018$, above the DLCA fractal dimension. For the average of the whole R_g vs N we see again a curved graph, with no possibility to define a fractal dimension, as shown in Fig. 9(d). As a final comment, we observe that the zone of scaling as a power law of R_{gz} vs N is in the region of elongated clusters shown in Fig. 9(a).

D. Cases for a quasi-DLCA regime only

If the Peclet number is very low, the clusters grow mainly by diffusion and sticking at contact. When they have grown large enough to drift downwards appreciably, they will remain with the same compacticity, unless they have the possibility to traverse enough distance in order to do a substantial sweeping of smaller clusters, which will increase its compacticity. However, if they do not traverse such distances, they will stay with almost the same DLCA fractal dimension, perhaps somewhat increased by the little sweeping they performed. These are the cases for which we have a quasi-DLCA regime only. As it was said, it is obtained with low P_e's; however, the shallower the depth, the higher the value of P_e that can be used to attain the regime. We have found a quasi-DLCA regime only for $Z=50\,000$ with $P_e=0.0001$; for $Z=5000$ with $P_e=0.0001$ and 0.001; and for $Z=500$ with $P_e=0.0001$, 0.001, and 0.01. In Fig. 10 we are showing the case $Z=500$ with the intermediate value of $P_e=0.001$. In Fig. 10(a) we can see that the anisotropy measure A_{yz} is practically one, taken into account the statistical uncertainties, in the whole range of sizes, with a similar plot for A_{xz}. In Fig. 10(b) we plot the average R_{gx} vs N, where we can see a well defined straight line between the arrows labeled "a." We have neglected the last four points corresponding to sizes for which we have a few clusters and hence the statistical uncertainties are higher, in order to have a better value for the scaling exponent. The inverse of the scaling power is $d_{fax}=1.847\pm0.007$. We have a similar plot for the average R_{gy} vs size, this time with $d_{fay}=1.840\pm0.011$. The average R_{gz} vs N is shown in Fig. 10(c), where we can see again a well defined straight line, now with $d_{faz}=1.839\pm0.008$. Finally, in Fig. 10(d) we show the whole average R_g vs N, where the straight line produced the following value $d_{fa}=1.848\pm0.005$. As the four inverses of the scaling powers are practically the same, up to the statistical uncertainties, we can say that for this case the cluster fractal dimension is $d_{fa}=1.848\pm0.005$, which is a little bit higher than the DLCA fractal dimension for this concentration [27,28].

E. The high Peclet number cases

We have found another behavior for which the clusters start to become immediately elongated along the z direction, the anisotropy measures A_{xz} and A_{yz} going down very fast, until they reach a minimum. Afterwards, they start to increase, crossing one at a certain size and ending up with oblate clusters. This occurs generally for high Peclet numbers; in fact, we have found this behavior with $P_e=1$ for all depths, and with $P_e=0.1$ for $Z=500\,000$. In these cases, the log-log plots of the average radii R_{gx}, R_{gy}, R_{gz}, and R_g are all curved, with no possibility to define a straight line. In Fig. 11

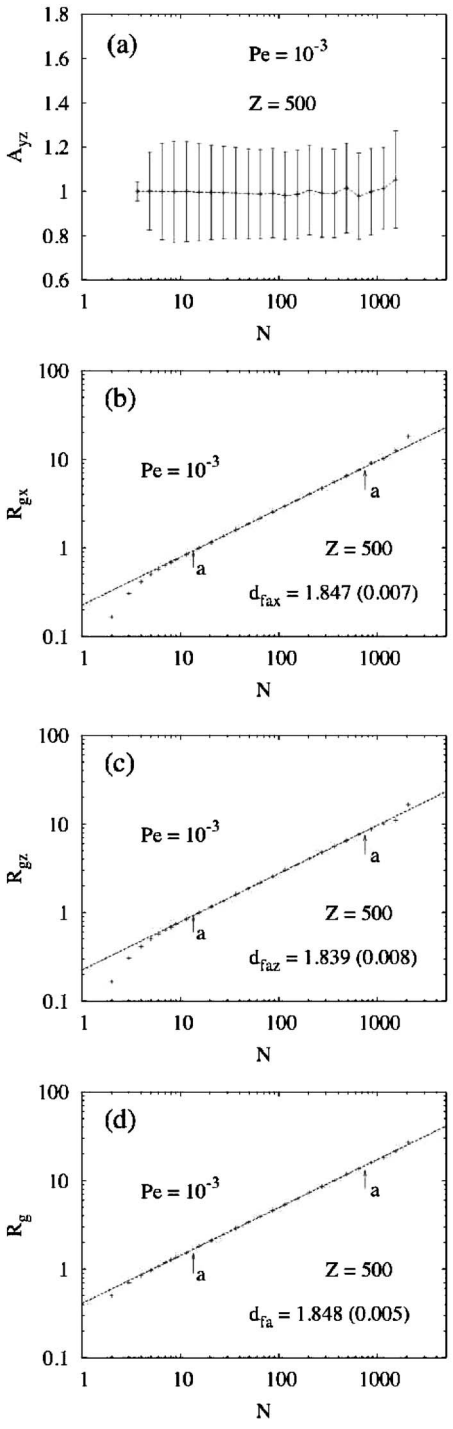

FIG. 10. All four figures correspond to the layer at $Z=500$ and $P_e=0.001$. (a) A plot of the anisotropy measure A_{yz} vs the size. (b) A plot of R_{gx} vs the size. (c) A plot of R_{gz} vs the size. (d) A plot of R_g vs the size.

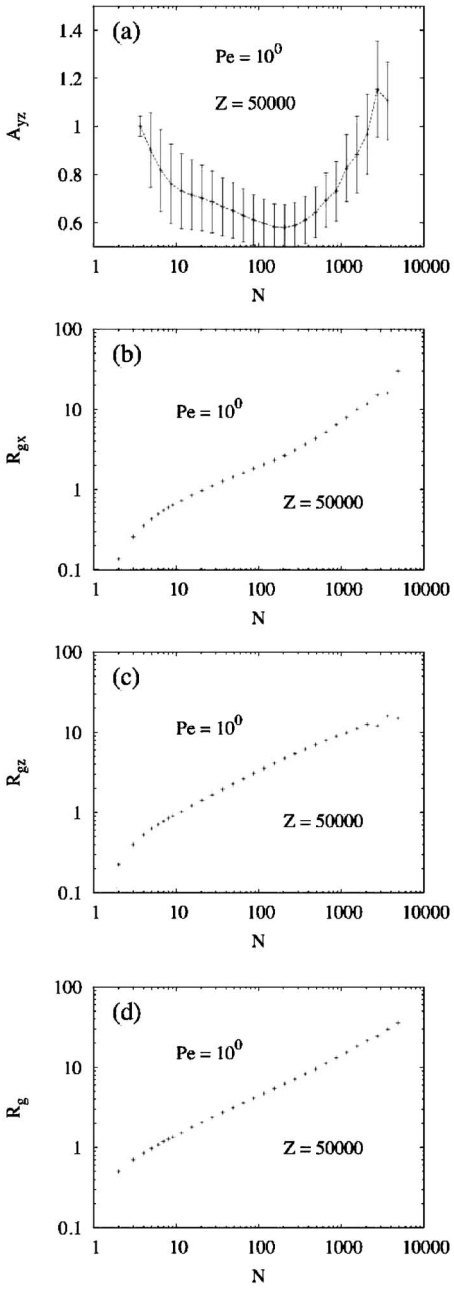

FIG. 11. All four figures correspond to the layer at $Z=50\,000$ and $P_e=1.0$. (a) A plot of the anisotropy measure A_{yz} vs the size. (b) A plot of R_{gx} vs the size. (c) A plot of R_{gz} vs the size. (d) A plot of R_g vs the size.

is shown the case for $Z=50\,000$ and $P_e=1$. As usual, we start first in Fig. 11(a) with one of the anisotropy measures, in this case A_{yz} vs N. As can be seen in the figure, A_{yz} goes immediately down, reaching values below 0.6 at the minimum, and then starts to increase crossing one at the size of around 2000, the clusters becoming oblate afterwards. The plot of A_{xz} behaves in a very similar way. The plot of the average R_{gx} vs N, shown in Fig. 11(b), is all curved as mentioned; therefore, there is no scaling as a power law of this quantity with N. Again, the behavior of the average R_{gy} vs N is quite similar to Fig. 11(b). In Fig. 11(c) we plot the average R_{gz} vs N, where we can see this time a continuous curvature, with no inflexion points. The absence of a straight line implies again that there is no scaling as a power law of R_{gz} with N. Finally, in Fig. 11(d) we are showing the plot of the average R_g vs N, which looks more straight than the previous two figures. Once more, this is an artifact coming from the fact that the average width goes up from a possible straight line, for large cluster sizes, while the average height goes down, making the total R_g to "almost" lie on a straight line. However, a closer inspection of the points and using the method of the moving boundaries, reveals the absence of a straight line in this figure also. As a conclusion, no fractal dimension can be defined in these cases of high P_e's.

V. CONCLUSIONS

As it was seen, it is possible to devise an algorithm to study the colloidal aggregation problem coupled with sedimentation, that can provide us with the *average* aggregation quantities at a fixed depth in the aggregating prism. The algorithm can be extended to the continuum, a work that is in progress. All this is particularly useful when studying big depths because, as we saw, it is for these depths that we can obtain the interesting case of a "sweeping scaling regime," for which we have self-similar large aggregates with a fractal dimension appreciably higher than the d_f of DLCA clusters. Otherwise, the task of performing *many* simulations in prisms of a *big* height, and obtaining the averages of the aggregation quantities over all the clusters, inside the layers at a fixed depth in the prisms of all the simulations, would become nearly hopeless. An interesting result coming from our simulations is that the aggregation quantities no longer depend on the height H of any confinement prism, but only on the depth Z at which they are measured, as long as $H \geq Z+\Delta/2$ of course.

The higher value of the d_f for the sweeping scaling regime comes, in our case, from the sweeping of the small clusters by the large settling ones, which in turn occlude the holes and cavities of these large aggregates, increasing in this way their compacticity. Note that we cannot invoke a restructuring mechanism for the large values of the d_f's, because it is not built-in in our model. Notice however that we found a lower fractal dimension (~ 2.05) for the settling clusters than the one found by the experimentalists (~ 2.2) [11]. It is conceivable that also a restructuring of the large clusters would make them still more compact, helping to push its d_f up to about 2.2. However, some other mechanisms could be present, such as a sticking probability lower than 1 (which would increase the d_f), the breakage of the clusters above a certain size (which may also increase their d_f), or the inclusion of the hydrodynamic interactions (whose effect on the d_f is unclear). As shown recently with the algorithm for which the lattice in the shape of a cube represented the whole prism [21], we can have a higher d_f for the settling clusters if we increase the concentration ($d_f \sim 2.2$ for $\phi=0.01$). We, however, preferred to use a concentration closer to the experimental one [9,11] to compare the results. An analysis of the concentration effects with the present, more correct algo-

rithm, in which the variations with depth are taken into account, should be done in the future.

The present problem is richer than the colloidal aggregation problem driven purely by diffusion in that (i) there are cases for which the average width and average height of the large settling clusters scale again as a power law with N, but with different scaling powers, obtaining in this case self-affine, anisotropic clusters. (ii) There are still some cases for which only the mean width *or* the mean height of the settling clusters scale as a power law with N, leading again to anisotropic clusters. (iii) There are further cases of high sedimentation strengths, for which neither the mean width nor the mean height of the settling clusters scale as a power law with N, which provides us also with anisotropic clusters. Finally, (iv) there are cases of very shallow depths and/or not so shallow depths but with low sedimentation strengths, for which a settling clusters regime disappears, leaving over only a quasi-DLCA regime. It should be mentioned that the anisotropies we found in cases (i), (ii), and (iii) could be blurred by the fragmentation of the aggregates in the experimental system, being perhaps valid up to the point where cluster breakage starts to occur. Although in cases (i), (ii), and (iii) we cannot define a clusters fractal dimension, we feel that they should be more "compact," in a still undefined way, than the DLCA clusters. This is because they are settling clusters that catch up with the smaller clusters below, which should occlude their holes and cavities, increasing in this way their compacticity.

We have confirmed the acceleration of the aggregation rate as compared to DLCA, due to the increasing pace at which the settling clusters drift downwards, forcing in this way an increase of the hitting rate. This speeding up of the aggregation rate is *followed* by a slow down when the "typical maximum size" clusters start leaving the layer, diminishing in this way the hitting rate. Afterwards, the layer deplenishes of smaller and smaller clusters, after a sufficiently long time.

As a final comment, we would like to point out the similarities of the present aggregation problem with the problem of droplet coalescence, of liquid droplets dispersed in another inmiscible liquid. Both theoretical and experimental studies [34,35] obtain a droplet size distribution that, at a given depth, initially shifts toward larger drop sizes due to coalescence, and then shifts back toward smaller drop sizes due to the larger drops settling or rising out of the dispersion because of sedimentation or buoyancy. The main difference with the present aggregation problem is the nonfractality of the aggregating (coalescing) objects. The theoretical descriptions of the drop coalescence process [34] are mainly based on population dynamics equations applied to the drop sizes, discretized into N discrete categories. It would be of interest to perform simulations of this process with a modified version of the present algorithm.

ACKNOWLEDGMENTS

The author is grateful to the Supercomputing Committee at UNAM for the CPU time granted. This work was supported in part by DGAPA-UNAM (PAPIIT Project No. IN118705-2).

[1] M. von Smoluchowski, Phys. Z. **17**, 557 (1916).
[2] M. von Smoluchowski, Z. Phys. Chem. (Leipzig) **92**, 129 (1917).
[3] T. A. Witten and L. M. Sander, Phys. Rev. Lett. **47**, 1400 (1981).
[4] P. Meakin, Phys. Rev. Lett. **51**, 1119 (1983).
[5] M. Kolb, R. Botet, and R. Jullien, Phys. Rev. Lett. **51**, 1123 (1983).
[6] *Kinetics of Aggregation and Gelation*, edited by F. Family and D. P. Landau (Elsevier, Amsterdam, 1984).
[7] S. K. Friedlander, *Smoke, Dust, and Haze: Fundamentals of Aerosol Dynamics*, 2nd ed. (Oxford University Press, New York, 2000).
[8] M. Couch, Ph.D. Thesis, Cambridge University, Cambridge, 1993.
[9] M. Wafra, Ph.D. Thesis, Université Paris-Nord, Paris, 1994.
[10] C. Allain, M. Cloitre, and M. Wafra, Phys. Rev. Lett. **74**, 1478 (1995).
[11] C. Allain, M. Cloitre, and F. Parisse, J. Colloid Interface Sci. **178**, 411 (1996).
[12] A. E. González and F. Leyvraz, in *Proceedings of the Statistical Mechanics in Physics and Biology Symposium of the MRS 1996 Fall Meeting*, edited by D. Wirtz and T. C. Halsey (Materials Research Society, Pittsburgh, 1997).
[13] D. Senis and C. Allain, Phys. Rev. E **55**, 7797 (1997).
[14] D. Senis, L. Gorre-Talini, and C. Allain, Eur. Phys. J. E **2**, 31 (2000).
[15] A. E. González, Phys. Rev. Lett. **86**, 1243 (2001).
[16] D. Senis, L. Gorre-Talini, and C. Allain, Eur. Phys. J. E **4**, 59 (2001).
[17] A. E. González, J. Phys.: Condens. Matter **14**, 2335 (2002).
[18] R. Leone, G. Odriozola, L. Mussio, A. Schmitt, and R. Hidalgo-Álvarez, Eur. Phys. J. E **7**, 153 (2002).
[19] G. Odriozola, R. Leone, A. Schmitt, A. Moncho-Jordá, and R. Hidalgo-Álvarez, Phys. Rev. E **67**, 031401 (2003).
[20] H. Wu, M. Lattuada, P. Sandkühler, J. Sefcik, and M. Morbidelli, Eur. Phys. J. E **19**, 10710 (2003).
[21] A. E. González, G. Odriozola, and R. Leone, Eur. Phys. J. E **13**, 165 (2004).
[22] M. Peltomäki, E. K. O. Hellén, and M. J. Alava, J. Stat. Mech.: Theory Exp. (2004) P09002.
[23] D. A. Weitz and J. S. Huang, in *Kinetics of Aggregation and Gelation*, edited by F. Family and D. P. Landau (Elsevier, Amsterdam, 1984), p. 19.
[24] D. A. Weitz, J. S. Huang, M. Y. Lin, and J. Sung, Phys. Rev. Lett. **54**, 1416 (1985).
[25] M. Y. Lin, H. M. Lindsay, D. A. Weitz, R. C. Ball, R. Klein, and P. Meakin, Nature (London) **339**, 360 (1989).
[26] M. L. Broide and R. J. Cohen, Phys. Rev. Lett. **64**, 2026 (1990).

[27] M. Lach-hab, A. E. González, and E. Blaisten-Barojas, Phys. Rev. E **54**, 5456 (1996).
[28] A. E. González, F. Martínez-López, A. Moncho-Jordá, and R. Hidalgo-Álvarez, Physica A **314**, 235 (2002).
[29] A. E. González, Europhys. Lett. **73**, 878 (2006).
[30] P. Wiltzius, Phys. Rev. Lett. **58**, 710 (1987).
[31] R. Botet and R. Jullien, J. Phys. A **19**, L907 (1986).
[32] P. B. Warren and R. C. Ball, J. Phys. A **22**, 1405 (1989).
[33] D. Fry, A. Mohammad, A. Chakrabarti, and C. M. Sorensen, Langmuir **20**, 7871 (2004).
[34] H. Wang and R. H. Davis, J. Fluid Mech. **295**, 247 (1995).
[35] H. Wang and R. H. Davis, J. Colloid Interface Sci. **181**, 93 (1996).